IL NUOVO CIMENTO **44 C** (2021) 1
DOI 10.1393/ncc/i2021-21001-2

COMMUNICATIONS: SIF Congress 2020

# Status of the FraISe facility and diagnostics system

N. S. MARTORANA(*)

*Dipartimento di Fisica e Astronomia "Ettore Majorana", Università degli Studi di Catania and INFN-LNS - Catania, Italy*

received 31 January 2021

**Summary.** — At Laboratori Nazionali del Sud of INFN (INFN-LNS), the upgrade of the Superconductive Cyclotron (CS) and the building of a new fragment separator, named FraISe (Fragment In-flight Separator), are currently ongoing. FraISe will permit to produce Radioactive Ion Beams (RIBs) with intensity in the range of $10^3$–$10^7$ pps, using the In-Flight Fragmentation method. The tuning and transport process of RIBs represents a critical step to deliver high-quality beams. This process can be very time-consuming and it needs a dedicated diagnostics system measuring features of RIBs. In this paper, the status of the FraISe facility as well as the related diagnostics system are discussed.

## 1. – Introduction

Nowadays, a challenge for nuclear physics is represented by the study of so-called exotic nuclei, namely unstable nuclei which lie far from the stability valley. The interest in this field of physics is due to unusual properties of exotic nuclei, which become useful to investigate nuclear structure models, the feature of the nuclear force and also nuclear reactions relevant for nuclear astrophysics. Among exotic nuclei features, the neutron excess in light neutron-rich nuclei leads to the formation of a nuclear halo. Exotic nuclei exhibit different halo structures as the di-neutron one, in which the halo is composed by two neutrons [1,2]. In the case of heavier neutron-rich nuclei, the neutron excess generally forms a neutron skin. This can be thought of as a mantle of almost pure neutron matter surrounding a stable core, in which neutrons and protons are approximately in the same number. The study of nuclei with a neutron skin is of particular interest, due to the presence of an excitation mode of the neutron excess against the nucleus core, known as Pygmy Dipole Resonance [3,4]. Both halos and skins determine a change in density, radii, and also in the shell structure with respect to the stable nuclei. Indeed, theoretical

(*) E-mail: `martorana@lns.infn.it`

models suggest that in exotic neutron-rich nuclei the known sequence of magic numbers breaks down, and a new shell model could be developed. This kind of investigations can be an useful tool also to add a further constraint to the knowledge of the Equation of State of nuclear matter. Indeed, the thickness of neutron skin is connected to the density dependence of the symmetry energy. In addition to neutron halo and skin, several data suggest the existence of a proton halo [2, 5]. However, the knowledge about proton halo nuclei remains still poor. Moreover, the study of clustering structure of $\alpha$ particles is a further important topic related to exotic nuclei, with outstanding impacts on the knowledge of the strong interaction [6]. Indeed, in the case of exotic nuclei, as beryllium or carbon isotopes, an evidence of neutron-$\alpha$ structure was underlined. As an example, in the case of $^{16}$C, three $\alpha$ particles are arranged in a linear or triangular structure while neutrons valence link two $\alpha$ particles, producing a rotational state [7]. Exotic nuclei also have an important link with nuclear astrophysics. Indeed, despite the fact that the energy production and nucleosynthesis in stars mostly occur through nuclear reactions between stable nuclei, exotic nuclei are implicated in different processes, as the r-process. Some stellar processes, such as supernovae explosions and stellar events at high temperatures and/or densities, often involve nuclear reactions including radioactive nuclei [8, 9]. In this framework, several facilities have been developed and upgraded worldwide with the aim to produce exotic beams [10-13]. Radioactive Ion Beams (RIBs) can be produced through two methods: the In-Flight Fragmentation method and the Isotope Separation On Line (ISOL) technique [14]. The advantage of the ISOL method is the quality of the beam, in terms of energy resolution and low emittance. On the other hand, the ISOL method is not advised for producing short-lived isotopes. The In-Flight Fragmentation method is based on the fragmentation of a stable beam, typically a heavy ion beam, on a thin target. In the case of peripheral nuclear reactions, exotic beams are formed with a forward focusing and are subsequently selected and transported with the use of a fragment separator and optical elements. This method has the main advantage to produce short-lived isotopes [15]. At INFN-LNS RIBs are produced employing this method, as described in detail in the following sections.

## 2. – FRIBs facility and diagnostics system

At INFN-LNS RIBs are produced, since 2001, using the FRIBs (in Flight Radioactive Ion Beams at LNS) facility through the In-Flight fragmentation method, employing a maximum beam power of 100 W. In detail, the FRIBs facility allows to produce exotic beams, in the range of intermediate energies, for ions from $^{6}$He to $^{68}$Ni, using the fragmentation of primary stable beams, accelerated by the Superconductive Cyclotron (CS), on a beryllium target placed at the exit of the CS [16-19]. The exotic beam, resulting from the fragmentation reaction, contains several stable and unstable isotopes. Therefore, the action of magnetic fields is necessary to select and transport the isotopes of interest for a specific investigation. The main selection occurs within a fragment separator, made of two 45° bending angle dipoles. The action of the magnetic fields permits to maximize the yield of the exotic beam of interest, reducing the presence of unwanted beams. Figure 1 (left) shows a map of the INFN-LNS, with the position of the fragment separator indicated by the ellipse and a photo of the beryllium target. However, a magnetic selection does not allow for the separation of isotopes with the same $A/Z$ ratio. Therefore, it is essential to proceed, event-by-event, with the characterization of beam components arriving on the target point, in order to off-line select the isotope of interest for the specific study [17]. For example, in the CHIMERA beam line the identification

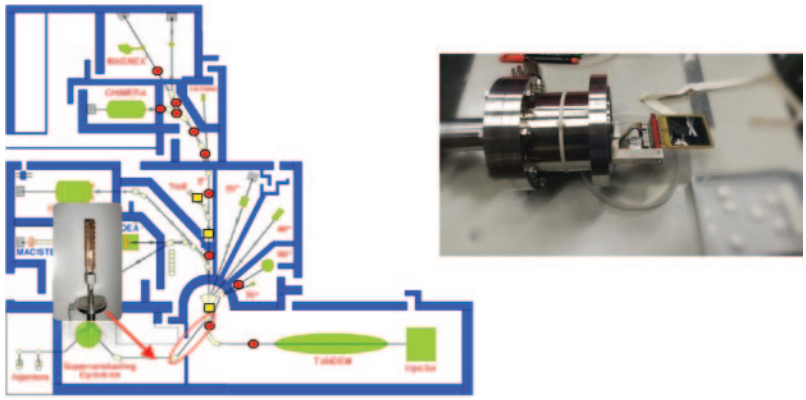

Fig. 1. – (Left) Map of the INFN-LNS. The dots represent diagnostics elements in which plastic scintillators are present. The squares represent diagnostics elements in which Double-Sided Silicon Strip Detectors (DSSSD) are present. The fragment separator is located inside the ellipse. The picture in the inset shows the $^{9}$Be target system. (Right) Picture of a DSSSD (140 $\mu$m) of the diagnostics system installed in the 0° experimental hall.

takes place through the $\Delta E$-TOF method, using a tagging system [20, 21]. This system consists of a Micro Channel Plate (MCP) detector that produces the start signal for the measurement of the Time Of Flight (TOF) and of a Double-Sided Silicon Strip Detector (DSSSD), which produces information about the energy loss, the position, and the stop for the measurement of the TOF. A PPAC (Parallel Plate Avalanche Counter) detector is also used to reconstruct the beam trajectory. Several measurements, concerning some of the aspects discussed in sect. **1**, have been performed using this facility [4, 7, 22, 23]. The main limitation of FRIBs is the maximum power delivered by the CS (100 W). Because of this, investigations have been focused on nuclei not far away from the stability

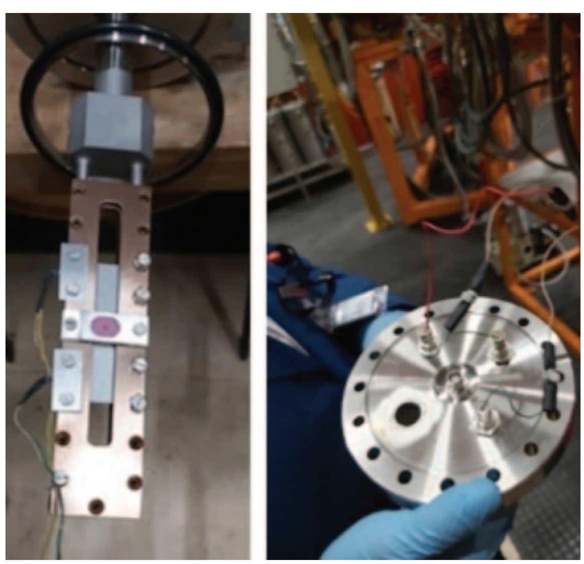

Fig. 2. – (Left) Photo of an alumina foil on the target holder. (Right) Photo of two PT100 thermic probes used to monitor the temperature of the target during the experiment.

valley, being the yields for very exotic nuclei not enough to carry out experiments with high statistics. Moreover, to achieve an optimal transport, from the production target (beryllium) to the final user point, one needs several diagnostics elements. In the FRIBs facility some of the diagnostics elements are made of plastic scintillators, which allow a measurement of the fragmentation beam total yield. The use of plastic scintillators is especially useful in cases where low intensities do not allow the use of traditional methods, such as the use of alumina coupled to optical cameras. In the past, silicon detectors were also used to determine the beam profile, reading the signal from the back side and the four corners, and applying a charge-sharing algorithm [24]. Recently, we proceeded with the installation and the test of new silicon detectors. The detectors installed are DSSSD made of $16 \times 16$ strips, each of them with $3 \times 48$ mm$^2$, see fig. 1 (right). Using these strip detectors, it is possible to obtain a reconstruction of the beam profile with a pixel resolution of $3 \times 3$ mm$^2$. In addition, through the identification technique $\Delta E$-TOF, in which the start signal is provided by the CS Radiofrequency signal (RF), it is possible to carry out an event-by-event identification. This allows to check the isotopic composition of the fragmentation beam along the beam line and not only in the final point. In specific cases, the use of a degrader, *i.e.*, a piece of matter placed at the dispersive focal plane between the two 45° dipoles, is possible in order to obtain a cocktail beam with a high purity of a specific isotope. Indeed, nuclei, depending mainly on their atomic number, will have different energy loss passing through the degrader. This means that nuclei with the same $A/Z$ will be separated in the second dispersive stage. In detail, the optical settings of the two dispersive sections of the fragment separator are not mirror of each other anymore and the magnetic rigidity of the second dipole has to be appropriately decreased. The purification technique, consisting in using the degrader, introduces further straggling and a loss of yield but it is advantageous if high-purity RIBs are required. The first purification test (TFD@LNS) was carried out at INFN-LNS in order to produce an exotic beam of $^{11}$Be with a high purity [25]. The $^{11}$Be exotic nucleus was produced using a primary beam of $^{13}$C, accelerated at 55 MeV/nucleon, impinging on a target of $^{9}$Be (1500 $\mu$m), and a homogeneous aluminum degrader (1000 $\mu$m), placed between the two 45° dipoles. Subsequently, an experiment, OTPC@LNS, was carried out at INFN-LNS, with the aim to study the $\beta$-delayed $\alpha$ decay of the $^{11}$Be nucleus, using an optical Time Projection Chamber (TPC) installed in the 0° experimental hall [26, 27]. For this goal, an exotic beam with high purity of $^{11}$Be was required. To reach this aim we used the same reaction and degrader employed in the TFD@LNS test. Since one of the crucial issues to get intense secondary beams is a narrow focusing of the primary beam on the production target, an alumina target was placed in an additional horizontal position of the production target system and watched by a camera (fig. 2 (left)). This allowed us to check and to optimize the focusing of the primary beam on the production target position. Moreover, the production target holder has been equipped with two PT100 thermic probes, as displayed in fig. 2 (right), that were used to monitor the temperature of the production target during operations. The thermic probes confirmed the quality of the cooling system, enough to dissipate the heat produced in the target by the impinging beam. In order to obtain a good transport of the beam, several diagnostics elements were installed and tested. A DSSSD detector (140 $\mu$m, $16 \times 16$ strips) was installed, at the exit of the fragment separator, before the main switching magnet, which represents one of the most crucial points for the transport of the beam. This diagnostics element permitted to optimize the production of RIBs. In order to check the quality of the performed selection, we installed a further 140 $\mu$m thick DSSSD at the entrance of the 0° experimental hall. We used the $\Delta E$-TOF technique for the event-by-event identification of the

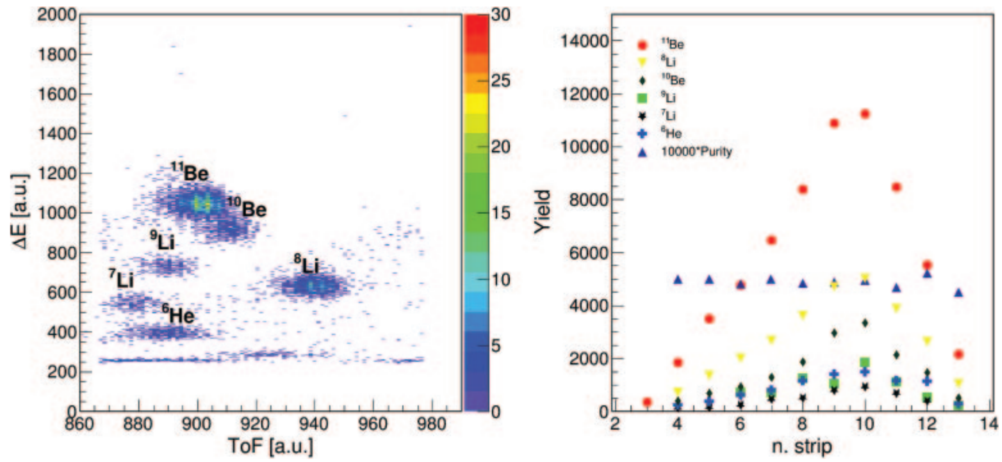


Fig. 3. – (Left) $\Delta E$-TOF plot related to a central strip of the DSSSD, obtained using a primary beam of $^{13}$C at 55 MeV/nucleon and a $^{9}$Be target, without the use of the degrader. (Right) Yields for several isotopes, obtained using a primary beam of $^{13}$C at 55 MeV/nucleon and a $^{9}$Be target, without the use of the degrader. The yields are displayed as a function of the DSSSD strip number, corresponding to a horizontal distribution (3 mm each point).

cocktail beam. The RF signal provided the start for the TOF measurement, while the strips of the DSSSD provided the stop signal, as well as the energy loss. Figure 3 (left) shows the $\Delta E$-TOF plot obtained without the degrader, using a $B\rho \approx 2.81$ Tm in both dipoles of the fragment separator to optimize the yield of $^{11}$Be. In this plot, we note the several isotopes that compose the cocktail beam. Without the degrader, we obtained a cocktail beam with a purity of $\approx$50% of $^{11}$Be, as it is also possible to observe in fig. 3 (right), in which we display the yields as a function of the DSSSD strip number, corresponding to a horizontal distribution (3 mm each point). Figure 4 displays the results

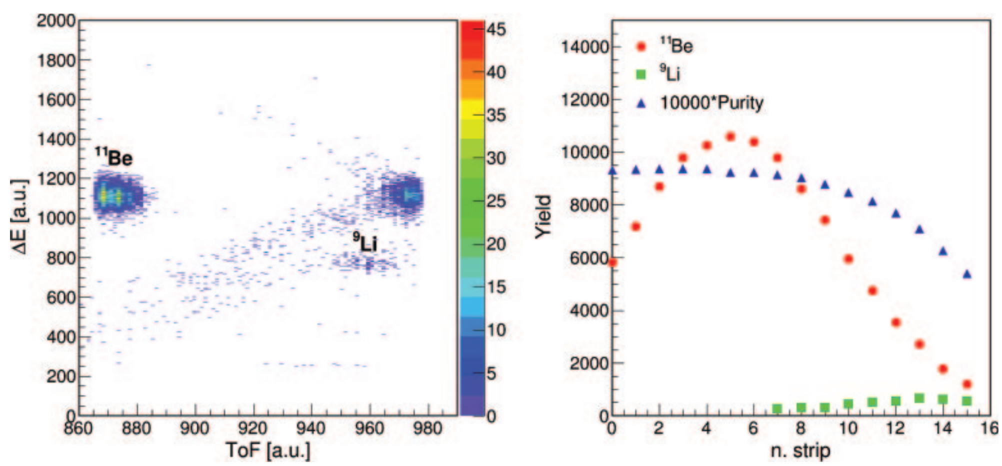


Fig. 4. – (Left) $\Delta E$-TOF plot, obtained using the same reaction of fig. 3 and the degrader. (Right) Yields, using the same reaction of fig. 3 and the degrader, obtained for several isotopes, as a function of the DSSSD strip number corresponding to a horizontal distribution (3 mm each point).

using the degrader, in this case the $B\rho$ of the second dipole was opportunely decreased at a value of ≈2.67 Tm, in order to optimize the yield of $^{11}$Be. In the $\Delta E$-TOF plot one can note the composition of the exotic beam, that in this case contains mainly $^{11}$Be with a low percentage of $^{9}$Li contaminant. This can be better appreciated in the right panel of fig. 4, in which we note an exotic beam with a purity of $^{11}\text{Be} > 90\%$. Finally, a diagnostics element, a DSSSD (70 $\mu$m, $16 \times 16$ strips), was installed before the TPC in the 0° experimental hall. The purpose of this diagnostics element was to check the yield and the beam profile before the TPC.

### 3. – FraISe@LNS-INFN and diagnostics system

The project of the Superconductive Cyclotron upgrade aims to provide stable ion beams with a power up to 10 kW [16, 17]. This will allow to obtain beams, for intermediate energies and for ions from carbon to argon, with intensity up to $10^{13}$ pps [17]. Currently, the building of a new fragment separator, named FraISe, is ongoing to exploit the capabilities of this CS upgrade for providing high-intensity exotic beams. The new facility will be installed in a new hall located in the region of the LS-20 and LS-40 experimental halls, as displayed in fig. 5 (left) [16, 17]. In the FraISe facility, due to radioprotection issues, the power of the primary beams will be limited to ≈2 kW. This value will permit to increase the yield by a factor 20 with respect to the FRIBs facility. The region that will host FraISe will be managed to allow a safe air treatment and an appropriate shielding of walls, floor and roof. The latter ones will be made with materials suitable for slowing down and absorbing radiations, mainly produced by neutrons and $\gamma$-rays, and to avoid a contamination in adjacent halls. Furthermore, a dedicated radio-

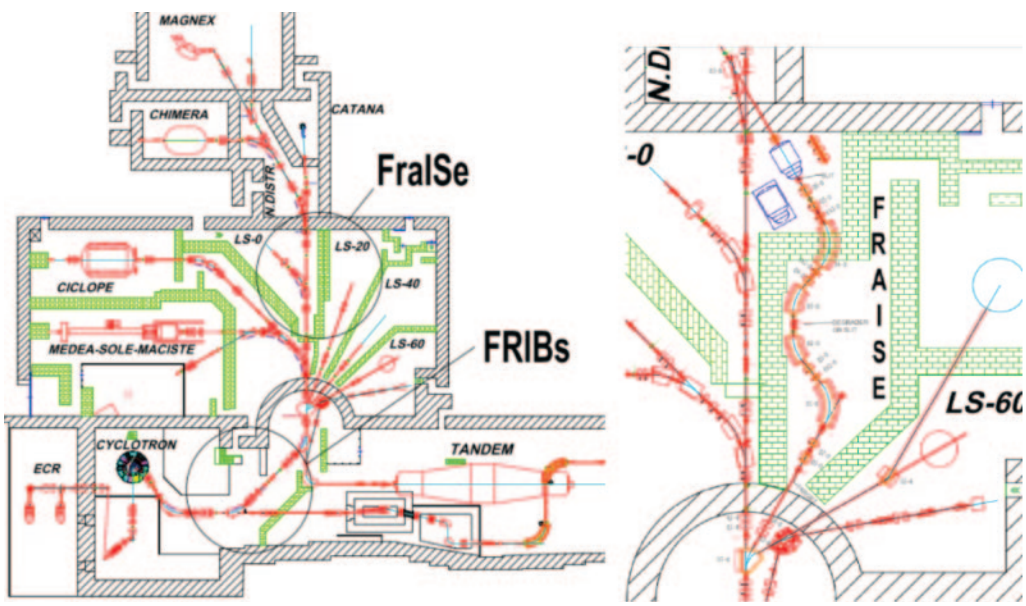


Fig. 5. – (Left) Schematic view of the INFN-LNS beam lines and halls. The positions of the FRIBs and FraISe facilities are indicated with circles. (Right) Scheme of the new fragment separator [16]. The blue chamber at the exit of the fragment separator is named GiRa.

protection system for the first magnetic dipole will be required. This dipole represents a crucial point, because the residual primary beam, stopped in the dipole, will deposit a high dose. Also a new production target, CLIM [28], will be used in the FraISe facility. Such target will be composed of a rotating system of circular beryllium or carbon targets, in order to increase the active surface and to avoid depositing the total intensity of the beam on a single spot. The target will be significantly activated, after and during experiments, and it will be impossible to remove it manually. For this reason, a remote control system will be used in order to automatically proceed with the replacement of the target and its storage. FraISe will be composed of four magnetic dipoles in a symmetric configuration, as shown in fig. 5 (right). The first part of the separator will be made of: two dipoles, placed at 70° and 40° bending angles, two duplets of quadrupoles, placed before and after the fragmentation target, and a quadrupole placed before the second dipole. The second part of the fragment separator will be a mirror-copy of the first one, in order to maintain the achromatic condition of the system. The system will allow to get a maximum value of $B\rho \approx$3.2 Tm. Moreover, two slits will be present in the facility: the first one will be placed in the dispersive plane, and the second one will be placed after the fourth dipole, in order to stop the undesired isotopes of the cocktail beam. Furthermore, the slit placed at the center of separator on the dispersive plane, where the value of energetic dispersion is high, will allow to vary the acceptance of $\Delta p/p$ of the fragment separator from typical values of $\Delta p/p \approx 1.2\%$ to lower values. After the central slit, it will be possible to insert an aluminum wedge/degrader, in order to perform a separation of ions with the same $A/Z$, following the procedure discussed in sect. **2**. Using FraISe it will be possible to deliver exotic beams towards the CHIMERA [20] and MAGNEX [29] halls. Moreover, the GiRA chamber will be also installed at the exit of the fragment separator, as shown in fig. 5 (right). The high beam intensity achieved with FraISe will not allow the full use of the tagging and diagnostics systems employed in the FRIBs facility. Therefore, an upgrade of the diagnostics system is also ongoing to meet the requirements of the FraISe facility. Indeed, the detectors will operate in a strong radioactive environment and in a wide intensity range, from $10^3$ pps, as typical for very exotic isotopes, to $10^7$ pps, as typical for exotic isotopes close to the stability valley. Moreover, the diagnostics system should be able to sustain several experiments per year. The diagnostics system will be versatile to allow its use both as a beam monitor and a tagging element, providing information about isotopic identification, energy, position and trajectory. In this framework, the system and skills developed with FRIBs, and discussed in sect. **2**, represent a reference study for the development of these systems. The RIBs composition will be investigated by measuring the $\Delta E$ energy loss of ions and TOF between two detectors, or with respect to a time signal synchronous with the primary beam arrival on production target, as the Cyclotron Radiofrequency signal. For the aforementioned reasons, we are investigating the possibility to use SiC detectors for the FraISe diagnostics system [30]. In detail, we are studying the building of an array of detectors based on SiC technology, where the single detection unity pad will be $4 \times 4$ mm$^2$ and 100 $\mu$m thick. By assembling an array of several pads it will be possible to cover $\approx 8 \times 4$ cm$^2$, enough for RIBs distribution in the high dispersion point. Such a segmentation will allow having no more than $10^6$ pps, even in the region where the beam profile is peaked. A feasibility study has already started, performing simulations and preliminary tests on the use of SiC detectors. In order to evaluate the possibility of using SiC detectors, we performed LISE++ simulations considering the configuration reported in ref. [16] and displayed in fig. 5 (right). In these simulations, we considered a primary beam of $^{18}$O at 55 MeV/nucleon, and a beam power of 2 kW on a $^9$Be target (1250 $\mu$m), in order to produce a $^{15}$C exotic nucleus. In the first case, we included a SiC detector, with thickness of 100 $\mu$m, placed after the exit slit (see fig. 5 (right)), setting an energy resolution of 0.5%. Figure 6 (left) shows the results of this simulation. In detail, this figure shows the spatial distribution of beam components, using a SiC detector placed after the exit slit. One can observe that the exotic beam contains mainly $^{15}$C isotope, with a purity of ≈60%, but also further isotopes are present ($^{12}$B,$^{17}$N,$^{10}$Be,$^{13}$B, etc.). For the sake of clarity, fig. 6 (left) shows only some of the main contaminants. In the second simulation, we included, with respect to the first simulation, a further SiC detector, 100 $\mu$m thick and with an energy resolution of 0.5%, placed after the central slit. Figure 6 (right) shows the simulation of the spatial distribution of beam components, using two SiC detectors, placed after the central and after the exit slit, respectively. In this case, one notes that the presence of the SiC detector, placed after the central slit, allows to purify the fragmentation beam with respect to the first configuration, obtaining a cocktail beam with ≈90% purity of $^{15}$C and a low percentage of contamination due to $^{13}$B and $^{17}$N isotopes. The simulation results allow to deduce that the presence of the SiC detector, placed after the central slit, is of relevant importance because it acts as an active wedge, increasing the $^{15}$C purity but keeping the $^{15}$C rate unchanged. This means that the detectors of such diagnostics system have to be uniform in thickness, since they will be also used as an active wedge. In order to obtain a more pure beam and to completely avoid other contaminants, it is possible to insert a passive Al wedge with an optimized thickness. Figure 7 displays the results of the simulation using a 200 $\mu$m Al degrader. In this case, the degrader introduces a further straggling but the yield is still high. Moreover, using the degrader we obtain a beam purity of $^{15}\mathrm{C} \approx 100\%$. Finally, using the $\Delta E$-TOF method in which the first SiC detector provides the start signal and the second SiC the stop and the energy loss, one can obtain the identification of the cocktail beam, as shown in fig. 8 (left). Figure 8 (right) shows the isotopic composition, using also the Al degrader. In this case, one can note the cleaning effect of the degrader, allowing to produce a beam with a high purity. Further simulations about several physics cases are discussed in ref. [31]. The energy resolution of the beam depends mainly on the $\Delta p/p$ value in the central slit. In the discussed simulations we used a constant value of $\Delta p/p \approx 1.32\%$. It is possible to improve this value, reducing the opening of the central slit, to produce a beam with a better energy resolution. However, this operation produces a loss in the production rate.

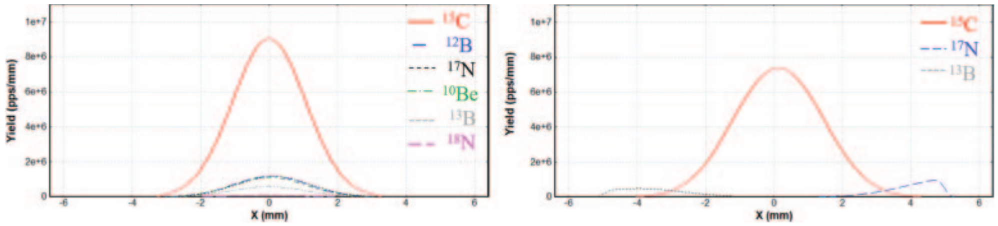


Fig. 6. – (Left) Simulation of spatial distribution of ions produced with FraISe, using a SiC detector placed after the exit slit. (Right) Simulation of spatial distribution of ions produced with FraISe using two SiC detectors (see text for details).

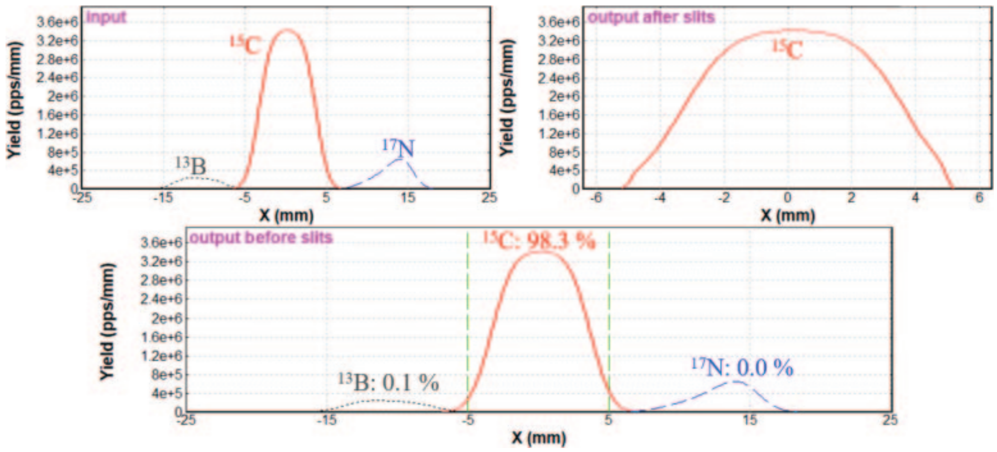


Fig. 7. – Spatial distribution of beam components, using two SiC detectors and an Al passive wedge. One can note the purification effect of the exit slit that removes the contaminants in input.

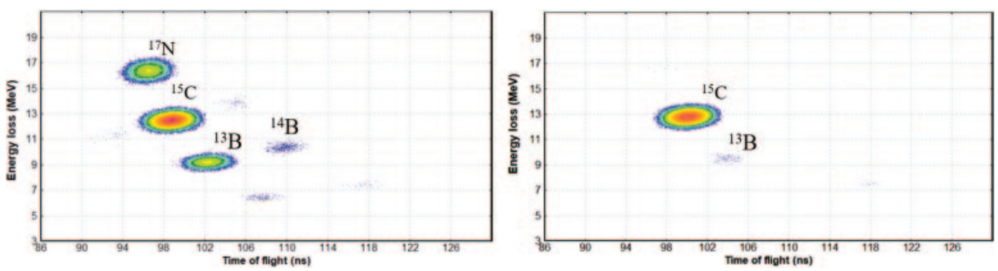


Fig. 8. – (Left) Simulation of $\Delta E$-TOF plot related to the production of $^{15}$C, without the use of Al degrader. (Right) Simulation of $\Delta E$-TOF plot related to the production of $^{15}$C, with the use of Al degrader. It is possible to note the effect of the presence of the Al wedge with respect to the case without wedge.

## 4. – Conclusion

In this paper, we reported the status of the FraISe facility and the related diagnostics system, presently in construction at INFN-LNS, in order to produce RIBs with high intensity and high quality. Preliminary investigations, performed both with tests and simulations, allowed to obtain a first reference study fixing the features of such diagnostics system. Further steps will concern the production of SiC arrays and the validation of the system, using both radioactive sources, low-energy stable beams and unstable nuclei. Moreover, in order to decrease the beam commissioning time and to allow a powerful control of the beam quality, also a fast integrated electronics, coupled to innovative software tools, based also on machine learning, is under development.

* * *

The author wishes to thank the NEWCHIM-CHIRONE Collaboration for the support to this work. Moreover, research reported in this publication was also partially supported by *Programma ricerca di ateneo UNICT 2020-22 linea 2*.

REFERENCES


[1] Tanihata I. *et al.*, *Phys. Rev. Lett.*, **55** (1985) 2676.
[2] Tanihata I. *et al.*, *J. Phys. G: Nucl. Part. Phys.*, **22** (1996) 157.
[3] Bracco A. *et al.*, *Prog. Part. Nucl. Phys.*, **106** (2019) 360.
[4] Martorana N. S. *et al.*, *Phys. Lett. B*, **782** (2018) 112.
[5] Minamisono T. *et al.*, *Phys. Rev. Lett.*, **69** (1992) 2058.
[6] Freer M. *et al.*, *J. Phys.: Conf. Ser.*, **381** (2012) 012009.
[7] Dell'Aquila D. *et al.*, *Phys. Rev. C*, **93** (2016) 024611.
[8] Decrock P. *et al.*, *Phys. Lett. B*, **304** (1993) 50.
[9] Belarge J. *et al.*, *Phys. Rev. Lett.*, **117** (2016) 182701.
[10] Anne R. *et al.*, *Nucl. Instrum. Methods A*, **257** (1987) 215.
[11] Geissel H. *et al.*, *Nucl. Instrum. Methods B*, **70** (1992) 286.
[12] Wei J. *et al.*, *Proceeding of HIAT18 Conference, Lanzhou, China, 22-26 October 2018*, (JACoW Publishing) 2019, p. 7.
[13] Kubo T. *et al.*, *Nucl. Instrum. Methods B*, **70** (1992) 309.
[14] Van Duppen P. *et al.*, *Isotope Separation On Line and Post Acceleration, The Euroschool Lectures on Physics With Exotic Beams, Vol. II*, edited by Al-Khalili J. and Roeckl E., *Lecture Notes in Physics*, Vol. **700** (Springer) 2006, pp. 37–77.
[15] Blumenfeld Y. *et al.*, *Phys. Scr.*, **T152** (2013) 014023.
[16] Russo A. D. *et al.*, *Nucl. Instrum. Methods B*, **463** (2020) 418.
[17] Russotto P. *et al.*, *J. Physics: Conf. Ser.*, **1014** (2018) 012016.
[18] Raciti G. *et al.*, *Nucl. Phys. A*, **834** (2010) 780c.
[19] Rapisarda E. *et al.*, *Eur. Phys. J. ST*, **150** (2007) 269.
[20] Pagano A. *et al.*, *Nucl. Phys. A*, **734** (2004) 504.
[21] Lombardo I. *et al.*, *Nucl. Phys. B Proc. Suppl.*, **215** (2011) 272.
[22] Raciti G. *et al.*, *Phys. Rev. Lett.*, **100** (2008) 192503.
[23] Acosta L. *et al.*, *Nucl. Instrum. Methods A*, **715** (2013) 56.
[24] Amato A. *et al.*, LNS Activity Report (2009).
[25] Martorana N. S. *et al.*, LNS Activity Report (2017–2018).
[26] Sokolowska N. *et al.*, LNS Activity Report (2019–2020).
[27] Martorana N. S. *et al.*, LNS Activity Report (2019–2020).
[28] Grévy S. *et al.*, contribution at the *24th World Conference of the International Nuclear Target Development Society-INTDS2008, Sep. 2008, Caen, France* (2008).
[29] Cappuzzello F. *et al.*, *Eur. Phys. J. A*, **52** (2016) 167.
[30] Tudisco S. *et al.*, *Sensors*, **18** (2018) 2289.
[31] Risitano F., *Produzione di fasci radioattivi con tecnica in-flight presso i LNS-INFN: stato e prospettive*, Tesi di Laurea Magistrale, Università degli Studi di Messina (2019–2020).